European Cells and Materials Vol. 12. 2006 (pages 81-91) DOI: 10.22203/eCM.v012a10 ISSN 1473-2262

BONE NANOSTRUCTURE NEAR TITANIUM AND POROUS TANTALUM IMPLANTS STUDIED BY SCANNING SMALL ANGLE X-RAY SCATTERING

M.H. Bünger[1,3,4], M. Foss[3,4,*], K. Erlacher[3,5,#], H. Li[2], X. Zou[2], B.L. Langdahl[1], C. Bünger[2], H. Birkedal[3,5], F. Besenbacher[3,4] and J.S. Pedersen[3,5]

[1] Department of Endocrinology and Metabolism C, Aarhus University Hospital, 2 Tage Hansens gade, DK-8000 Aarhus, Denmark
[2] Ortopaedic Research laboratory, Aarhus University Hospital, 44 Nørrebrogade, DK-8000 Aarhus, Denmark
[3] Interdisciplinary Nanoscience Center (iNANO), University of Aarhus, Ny Munkegade, DK-8000 Aarhus, Denmark
[4] Department of Physics and Astronomy, University of Aarhus, Ny Munkegade, DK-8000 Aarhus, Denmark
[5] Department of Chemistry, University of Aarhus, 140 Langelandsgade, DK-8000 Aarhus, Denmark
present address: Bruker AXS Inc., 5465 E. Cheryl Parkway, Madison, WI 53711, USA

Abstract

Bone sections including either titanium or porous tantalum implant devices used for interbody spinal fusion were investigated with position-resolved small angle X-ray scattering (sSAXS). The samples were obtained from six-month-old pigs that had undergone surgery three months prior to sacrifice. The aim of the study was to explore the possibility of using sSAXS to obtain information about thickness, orientation and shape/arrangement of the mineral crystals in bone near the implant surfaces. Detailed sSAXS scans were carried out in two different regions of bone adjacent to the implant in each of the implant samples. In the implant vicinity the mineral crystals tended to be aligned with the surface of the implants. The mean crystal thickness was between 2.1 and 3.0 nm. The mineral crystal thickness increased linearly with distance from the implant in both regions of the porous tantalum implant and in one of the regions in the titanium sample. In the second region of the titanium sample the thickest mineral crystals were found close to the implant surface. The observed differences in mineral thickness with distance from the implant surfaces might be explained by differences in mechanical load induced by the implant material and the geometrical design of the implant. The study shows that sSAXS is a powerful tool to characterize the nanostructure of bone near implant surfaces.

Key Words: Small angle X-ray scattering, biocompatibility, orthopaedic implants, bone ultrastructure, biomineralization.

Address for correspondence:
Morten Foss
The Interdisciplinary Nanoscience Center (iNANO), University of Aarhus
Building 1522, Ny Munkegade
8000 Aarhus C, Denmark
Telephone Number: +45 89 42 36 98
FAX Number: +45 86 12 07 40
E-mail: foss@inano.dk

Introduction

The formation of bone around the implant is the basis for the long-term mechanical fixation of the implant *in vivo*. When new orthopaedic implant devices are tested in animal models prior to clinical use in humans, the integration of the implant in bone is typically evaluated using various laboratory tests such as histomorphometry, micro-CT analysis and mechanical tests (Melsen and Steiniche, 1993; Gefen, 2005). These methods provide useful information about bone in-growth into and around the implant surface on a micrometer length scale and about the mechanical stability of the bone/implant integration; both of which are relevant parameters for the evaluation of the capabilities of the implants. However, these techniques do not offer direct information on the length scale of the bone matrix constituents, like collagen fibres and carbonated hydroxy apatite crystals (HA), which have structural features within the 1–100 nm length scale (Mann, 2002).

During bone formation, osteoblasts produce a mineralizable organic bone matrix rich in collagen type I that is subsequently mineralized under the influence of non-collageneous matrix proteins (Young, 2003). The mineralization of the organic bone matrix results in the formation of plate shaped HA crystals with dimensions of the order of 40×10×2.0-3.0 nm (Mann, 2002). Most of the HA plates are located in close connection to the collagen type I fibres with the long plate dimension oriented in the direction of the collagen fibres (Landis, 1999). The process of bone formation around an implant is affected by several factors including the implant material, mechanical load, growth factors and hormones (Albrektsson and Johansson, 2001). However, further insights into the extent to which these factors influence the structure of bone on the nanometer length scale around implants is needed. It is conceivable that the structure of bone at the nanometer length scale reflects both the chemical, mechanical and geometrical properties of the implant and the local environment around the implant *in vivo*. Non-destructive techniques probing the nanometer length scale is therefore required. Small angle X-ray scattering (SAXS) is the technique of choice, which offers unique information about the thickness, orientation and shape of the mineral plates (Fratzl *et al.*, 1991; Fratzl *et al.*, 1992; Fratzl, 1994; Fratzl *et al.*, 1996). We have previously shown that the SAXS technique can be used

to measure the growth of HA mineral plates during endochondral ossification and provide structural information about the unmineralized fibrous tissue (Bünger *et al*., 2006). Here, we apply position-resolved scanning SAXS (sSAXS) to gain information about the nanostructure of bone around two implant devices with significantly different properties. The two implants are made of titanium (Ti) and porous tantalum (Ta), respectively. These materials are commonly used for bone implants in joint replacement applications, because both materials are biocompatible and bone conductive (Albrektsson and Johansson, 2001; Bobyn *et al*., 2004). With respect to spinal surgery, these properties have resulted in the development of implant devices for interbody spinal fusion. The investigated bone-implant specimens were obtained from two previous studies, where different types of spinal implants devices were experimentally tested in an anterior interbody lumbar spinal fusion model in pigs (Zou *et al*., 2004; Li *et al*., 2005). Both devices have a central hole allowing bone to grow through the implant and that thereby enhancing osseous integration. The Ta implants has a porous wall structure that provide additional tissue integration (Zou *et al*., 2005; Bobyn, 1999; Bobyn *et al*., 1999). The pores make up about 70% to 80% of the wall volume and have an average pore size of 400 to 500 μm. They are fully interconnected and result in an implant with a stiffness similar to the one found in trabecular bone (Bobyn *et al*., 1999). Some of us previously found that the Ti and porous Ta implants provide solid spinal fusion in 80-90% of the cases (Zou *et al*., 2004; Li, 2004; Li *et al*., 2005, Zou *et al*., 2005). However, the porous Ta has the advantage of requiring a smaller amount of bone graft in the central hole of the implant. Here, we extend the clinical studies by investigating the nanostructure of bone near two representative implant samples. The aim of the present study is to explore the possibility of using sSAXS to characterize the organization of crystallites and molecules in bone near and around the implants. A detailed understanding of the ultrastructure of bone around and near implants, and how this is related to the implant properties, may in the long term provide inspiration for the development of new implant materials.

Materials and Methods

Samples

The samples were obtained from our previous studies (Zou *et al*., 2004; Li *et al*., 2005). Briefly, the spinal implants of Ti and porous Ta were inserted into two different three-month-old Danish landrace pigs weighing approximately 50 kg. The implants were filled with bone graft from the iliac crest and inserted into the intervertebral disc space at different levels of the lumbar spine according to the experimental design. The pigs were sacrificed at the age of six months, and the lumbar spine including the implants was obtained. The specimens were dehydrated in a graded series of ethanol (70% to 96%) containing 0.4% basic fuchsin, which stains anionic structures in reddish colours, and embedded in poly-methylmethacrylate (PMMA).

For histological analysis and SAXS, parallel sections with a thickness of approximately 40 and 190 μm, respectively, were cut using a KGD 95 sawing microtome (Meprotech, Heerhugowaard, Netherlands). Since the thickness of the SAXS sections did not allow proper light microscopy imaging, sections parallel to the SAXS samples were used for histology. Prior to imaging, the sections for histological analysis were counterstained for bone with 2% light green for two minutes.

sSAXS setup

The experiment was performed on a modified SAXS Nanostar (Bruker-AXS GmBH, Germany) (Pedersen, 2004) using an X-ray generator with a rotating copper anode (45 kV / 90 mA; Cu-*K*a, $\lambda = 0.154$ nm). The scattered photons were collected by a Bruker AXS HI-STAR position-sensitive area detector. The direct X-ray beam was blocked by a beam stop (Ø=3.0 mm) placed in front of the detector. The implant samples were mounted in a motorized sample holder, which allowed scanning of the sample in the X-ray beam with a precision better than 0.1 μm in the horizontal (x) and vertical direction (y). The diameter of the X-ray beam at the sample position was 100 μm. Consequently, all data correspond to the average over a specimen volume laterally defined by the diameter of the X-ray beam. In all scanning experiments, the step width in the x and y directions was 50 μm to allow distinguishing variations at distances smaller than the beam diameter.

Both survey X-ray transmission and SAXS intensity scans were conducted on each sample with a measurement time of 1 s/point. The transmission scan was carried out by placing a uniform strongly scattering specimen (glassy carbon) right after the bone sample. In this case the integrated scattering intensity is proportional to the transmission of the X-ray through the bone and/or implant.

Following the initial scans, detailed investigations were made of seven and ten different regions in the Ti and Ta implant sample, respectively. The number of recorded SAXS 2D frames was approximately 1000 frames in each of the implant samples. Here, we discuss results from two representative regions in each of the samples; the other areas displayed similar behaviour. In order to improve the statistics of this investigation, the measurement time was increased to 100 s per point. Data points without bone or fibrous tissue were excluded using a filter variable based on the integrated SAXS intensity. The remaining data analysis and visualization was done using home written Matematica5® routines.

SAXS data evaluation

The X-ray beam is scattered by variations in the electron density of the sample on the nanometer length scale. In the bone, the variation in electron density is mainly due to differences in electron density between inorganic minerals and organic molecules. In this good approximation the SAXS technique offers unique information about mineral particle thickness, T, orientation and shape (Fratzl *et al*., 1991; Fratzl *et al*., 1992; Fratzl *et al*., 1996; Rinnerthaler *et al*., 1999). The SAXS data were analyzed, and these parameters were determined using a previously described procedure (Bünger *et al*., 2006). Here, a brief summary is given. The scattered intensity is a function of the scattering

angle, 2θ, and the azimuthal angle, χ, that is the angle extending around the incident X-ray beam. The length of the scattering vector, *q*, is related to the angle by:

$$q = \frac{4\pi \sin\theta}{\lambda}$$

$I_q(\chi)$ and $I(q)$ were calculated from the 2D spectra by integration from q_{min} = 0.00966 Å^{-1} and q_{max} = 0.3484 Å^{-1} for $I_q(\chi)$ and by averaging over the full 360° of χ for $I(q)$.

The presence of oriented structures, e.g., mineral crystals in bone, in the volume interacting with the X-ray beam results in a SAXS pattern that is not radially symmetric around the direct beam; an azimuthal dependence directly related to the predominant orientation of the mineral plates is obtained (Fig. 1A). This azimuthal dependence of the intensity can be determined from the radially integrated intensity, $I_q(\chi)$. In the region of bone, the $I_q(\chi)$-distributions have two symmetrical peaks separated by 180° (Fig. 1B). In an automated procedure using a home-written analysis program, each $I_q(\chi)$ curve was fitted with two Gaussians curves with the same height and width and separated by 180° plus a constant background. We have used the direction of the long axis of the HA plates, which is parallel to the crystallographic *c*-axis, to indicate the predominant orientation. Furthermore, a parameter describing the projected degree of orientation, *PDO*, of structures within the probed sample volume can be obtained from the ratio of the intensity of the two Gaussians curves and the total scattering intensity. Note that both the predominant orientation and degree of orientation should be regarded as the 2D projection of the particles perpendicularly to the beam (Rinnerthaler *et al.*, 1999).

The scattering vector modulus, *q*, reflects the typical length scale in the investigated material $\xi \approx \pi/q$. Thus, information about the particle shape and characteristic thickness is obtained from different domains of the SAXS intensity averaged over the azimuthal angle, $I(q)$ (Figure 1C). The particle shape can be described by the shape parameter, α, which is determined from power-law fits ($I(q) = Aq^{-\alpha}$) to the *q* region between 0.015-0.06 Å^{-1} in the present case. The shape parameter, α describes the shape and relative arrangement of the minerals in bone. For example, needle-shaped and plate-like particles show α = 1 and α = 2, respectively. The magnitude of α is thus directly related to the dimensionality of the particles considered. For non-integer values of α, the particles are termed fractals of dimensionality $d_f = \alpha$ (Poon and Haw, 1997). The higher the value of d_f, the more dense and compact is the structure of the bone.

In the high-*q* range the scattering intensity follows the Porod behaviour $I(q) = Pq^{-4}$, for all types of particles with a sharp surface, where *P* is the Porod constant (Lindner and Zemb, 2002). For a two-phase system the Porod region provides information about the total interface area. In the present case, the Porod region was found at $q > 0.20$ Å^{-1}. The mineral crystal thickness, *T*, was obtained from

$$T = 4\int_0^\infty q^2 I(q)dq / (\pi P)$$

(Poon and Haw, 1997). *P* was determined by fitting $I(q) = Pq^{-4}$ to the data, while the integral

$$\int_0^\infty q^2 I(q)dq$$

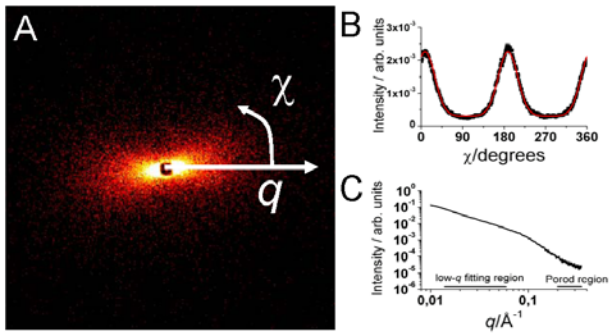

Figure 1. (A) Example of a raw 2D SAXS image from the position of the upper left frame in Figure 3: Ti-2. *q* and χ are the scattering vector and azimuthal angle, respectively. (B) The SAXS intensity plotted as a function of the azimuthal angle, χ. The red line displays the fit with the double Gaussian function. (C) The SAXS intensity averaged over the azimuthal angle, $I(q)$. Correction for shadowing by the beamstop has been made in the *q*- region below 0.02 Å^{-1}.

was evaluated numerically in the *q*-range q_{min}-q_{max}. The contributions outside this range were calculated analytically by extrapolating in the following manner: $I(q) = I(q_{min})$ for $q < q_{min}$ and $I(q) = Pq^{-4}$ for $q > q_{max}$. For two-phase systems with sharp interfaces (like mineral particles embedded in collagen), *T* describes the volume to surface ratio of the particles without any assumptions about shape (Rinnerthaler *et al.*, 1999). Specifically, if the particles are plate-like, the *T* parameter is a measure of the mean thickness (Fratzl, 1994).

Results

Histology

Optical microscopy images of the Ti and Ta sample are shown in Figures 2A and 2B, respectively, while Ti-1', Ti-2', Ta-1' and Ta-2' are high magnification images of positions corresponding to the ones studied in detail by SAXS. Bone (green) in-growth accounted for approximately 2/3 of the cage height in the Ti implant sample (Fig. 2A), while new bone bridged the central hole completely in the Ta implant (Fig. 2B). In the Ti sample the central hole of the implant was only partly bridged by bone and a gap without bone was found in a large region between the two columns of in-growing bone. Futhermore, a gap between bone and implant was observed in several regions (Fig. 2A). This situation was similar to our previous observations for this type of implant, and is most likely due to shrinkage of the tissue in the fixation process (Li, 2004). In the Ta sample no gap between bone and implant was observed, and it was apparent that bone grows into the porous Ta implant material (Fig. 2B). In both implant samples, bone was especially present at positions along the edges of the implant. The bone graft inserted in the hole of the two cages during surgery cannot be observed in the two samples and is most likely completely resorbed.

sSAXS - Ti sample

Figure 3A shows the integrated intensity of the transmitted X-ray signal of the Ti implant sample. The attenuation of the intensity of the transmitted X-rays by the sample was proportional to the electron density of the sample at the position probed. Low X-ray transmission was therefore found in the regions with high electron densities, e.g. of implant and bone (black, no transmission). This was in contrast to the positions of bone marrow cavities, and the gaps between bone and implant where high transmission was found due to the low electron density of the PMMA support. Figure 3B displays the integrated SAXS intensity, which originates from nanometer scale variations in electron density. A high SAXS signal was found in the regions of bone due to differences in electron density between the organic matrix and the inorganic crystallites. Low SAXS intensity was found at the positions of implant material and in the bone marrow cavities. The observed scattering properties of bone were consistent with previous observations (Fratzl *et al.*, 1991; Fratzl *et al.*, 1996, Bünger *et al.*, 2006). The two areas marked with Ti-1 and Ti-2 in Figure 3A represent regions of which detailed scans were performed. Ti-1 is located at the superior side of the implant towards the vertebral bone (*n*=273 points), while Ti-2 aligns the implant surface inside the central hole of the implant and (*n*=173 points).

The average *PDO* was 27.0 ± 16.4% and 34.1 ± 15.1% (mean ± standard deviation (SD)) in Ti-1 and Ti-2, respectively (Table 1). The predominant orientation of the mineral particles in Ti-1 was parallel to the implant surface (Fig. 3: Ti-1 – *PDO*). However, the predominant orientation changed significantly within approximately 100 µm from the implant surface, coinciding with low *PDO* values and the particles being predominantly aligned perpendicular to the implant plane. In contrast the predominant orientation was approximately parallel to the surface throughout the thickness of the bone investigated in region Ti-2 (Fig. 3: Ti-2 – *PDO)*.

Panels Ti-1 – *T* and Ti-2 - *T* of Figure 3 illustrate the thickness parameter *T* by the colour code. In Ti-1, the mean *T* was 2.50 ± 0.17 nm (mean ± SD), while it was 2.43 ± 0.16 Å in Ti-2 (Table 1). High values of *T* of approximately 2.7–2.8 nm were found close to the implant surface in Ti-1, especially in the lower and right part of the investigated region (Fig. 3: Ti-1-*T*). In contrast to this, the smallest values of *T* in Ti-2 were found close to the implant, with values of around 2.2–2.3 nm (Fig. 3: Ti-2 -*T*). The shape parameter, α, ranged from 1.6 to 2.2 in Ti-1 (Fig. 3: Ti-1 – α) and 1.8 to 2.2 in Ti-2 (Figure 3: Ti-2 -α,) (Table 1). Interestingly, in Ti-1 low values of α around 1.6-1.7 were found in the region of bone approximately 100 µm, where also low PDO values and change in predominant crystal orientation were found.

To look for systematic variations in *PDO* and *T* with the distance from the implant surface, we calculated the average value of these parameters as a function of the shortest distance to the surface. No systematic trends in the averaged value of *PDO* were found in the data corresponding to area Ti-1 in Figure 3. The averaged *PDO* ranged from 16.7 ± 2.6 % (average ± standard error of mean (SEM)) to 39.1 ± 4.2 % at distances 150-200 µm and 600-650 µm from the implant surface, respectively (Fig. 4A). Lower values tended to be closest to the implant surface. In Ti-2 a strong linear increase in *PDO* from 29.4 ± 4.6 % to 44.0 ± 4.0 % over a distance of 500 µm (linear regression analysis: $R = 0.93$, $P<0.0001$) was observed (Fig. 4B).

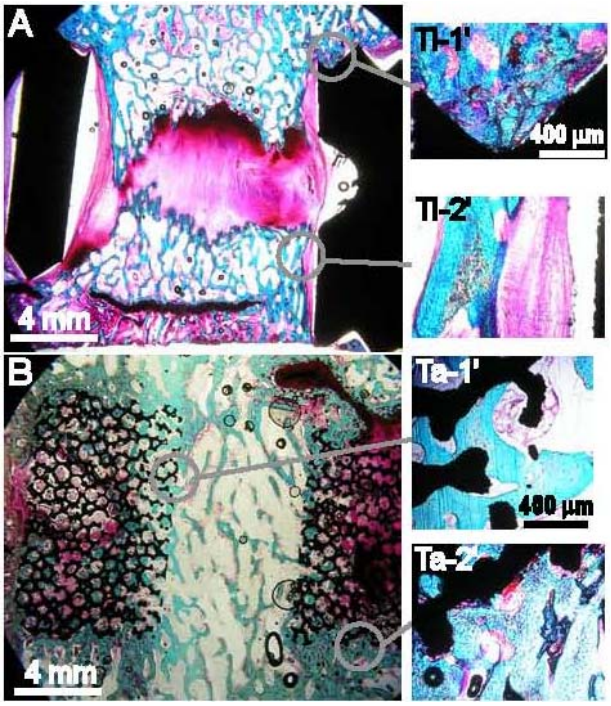

Figure 2. Optical micrographs of the Ti implant sample (A) and the Ta implant sample (B) (basic fuchsin and light green staining). The sections are parallel to the ones used for the SAXS measurements. Ti-1', Ti-2', Ta-1' and Ta-2' correspond to the positions of which detailed SAXS investigations were performed.

The *T* vs. distance to implant surface-plot shows the highest values of *T* close to the implant surface in Ti-1 (Fig. 4C). For the positions within 0–50 µm of the surface, *T* was around 2.72 ± 0.04 nm (average ± SEM). From the implant surface and outward *T* decreased to 2.38 ± 0.01 nm at a distance of 300-400 µm and then increased slightly to approximately 2.45 ± 0.01 nm around 600 µm from the surface. In Ti-2 a linear increase in *T* with distance from the implant was found (Fig. 4D) (linear regression analysis: $R = 0.98$, $P < 0.0001$). The increase in *T* ranged from 2.20 ± 0.04 nm to 2.57 ± 0.03 nm over the distance from 400 to 950 µm from the implant surface.

sSAXS - Ta sample

Survey scans of the Ta sample are shown in Figs. 5A (transmitted X-ray intensity) and 5B (integrated SAXS signal). Detailed scans were made of the areas marked with Ta-1 and Ta-2 in Figure 5A. Area Ta-1 was within the hole in the implant (*n*=213), while Ta-2 was at the bottom side of the implant (*n*=281). The complicated geometry made a determination of the exact position of the implant surface uncertain, however general trends could be extracted. The predominant orientation of the particles tended to be parallel to the implant surface in both regions (Fig. 5: Ta-

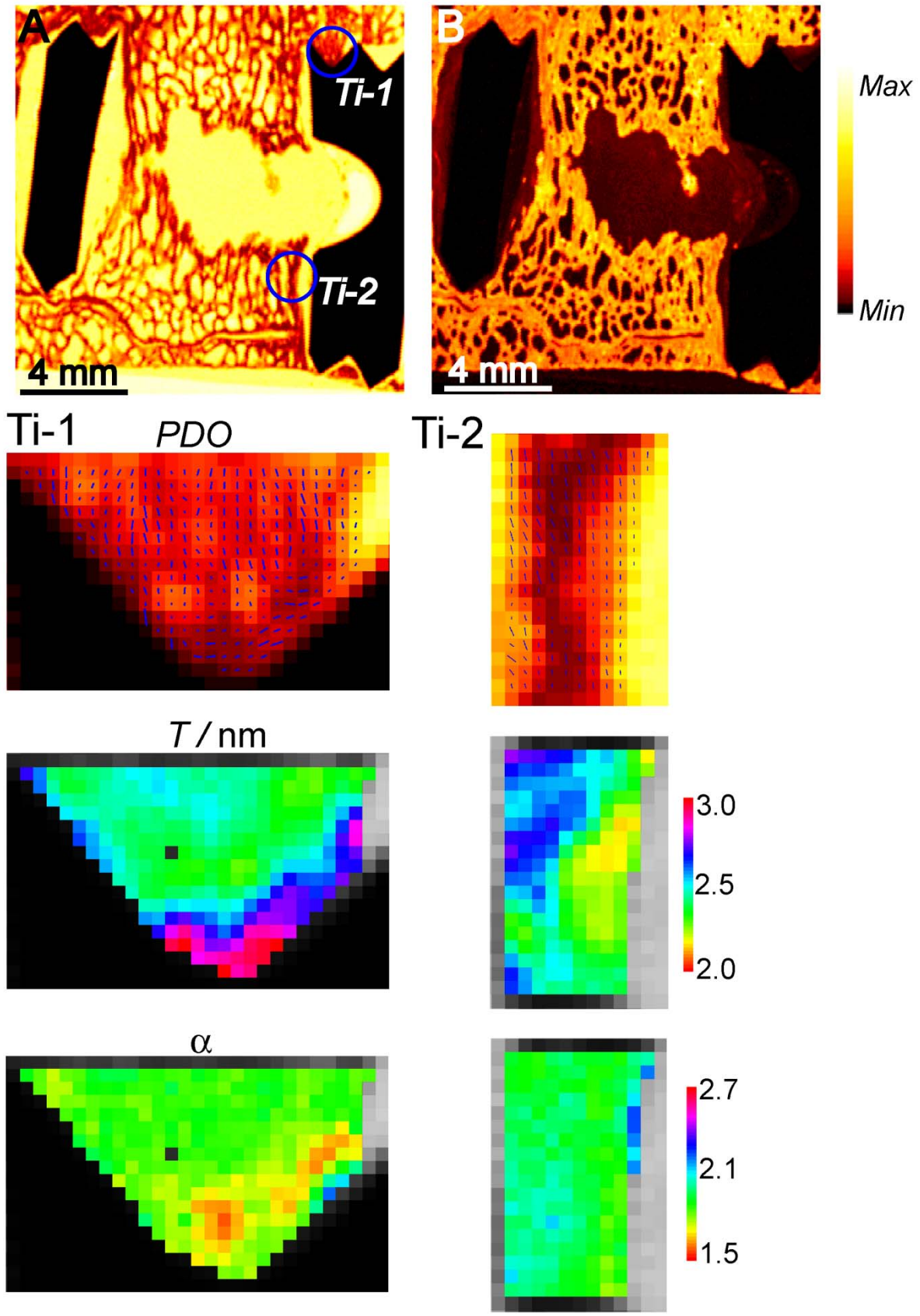

Figure 3. sSAXS images of the Ti implant specimen. The pixel size is 50 µm in all images. (A) Survey X-ray transmission scan. (B) Survey SAXS intensity scan showing the integral SAXS intensity. Ti-1) and Ti-2) Detailed investigations of two regions of bone facing the implant, marked in A. The background in the plots of *PDO*, *T* and α maps the X-ray transmission. *PDO*: The projected predominant orientation of the particles is indicated by the direction of the blue lines. The length of the blue lines is proportional to the *PDO* of the mineral particles. One pixel width equals a *PDO* of 83%. *T*: mean thickness of the apatite plates. α: The colour equals the magnitude of the shape parameter.

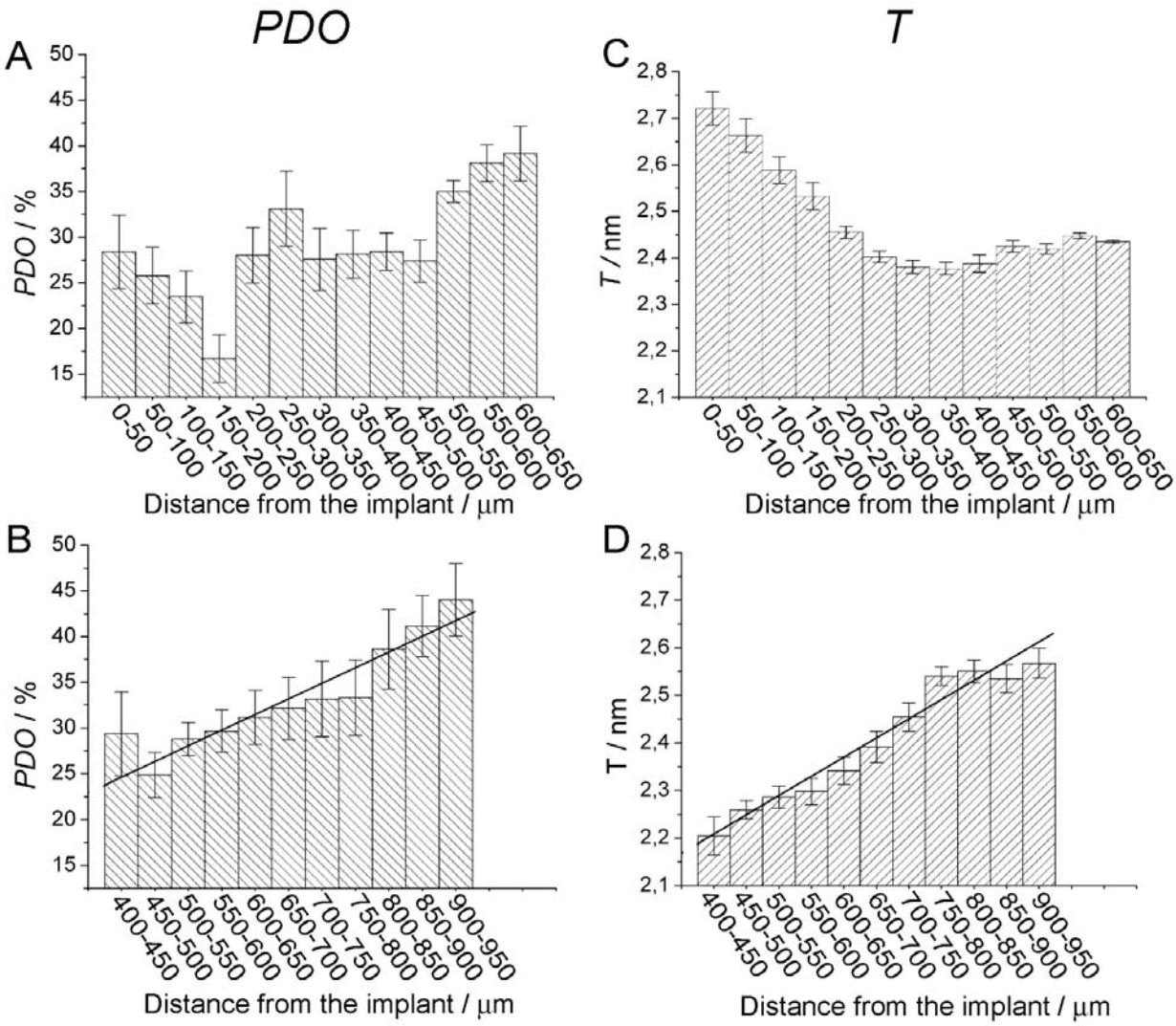

Figure 4. Ti sample. The average *PDO* (A, B) and *T* (C, D) shown as a function of the shortest distance from the implant surface. The solid bars are mean values, while the error bars are the uncertainty around the mean. Trend lines are shown for significant linear correlations ($p < 0.05$). The graphs (A) and (C) represent the Ti-1, while (B) and (D) denote Ti-2 (Fig. 2). For the region Ti-2 there might be an offset in the measured distance from the implant because of shrinkage in the fixation process. The measured distance from the implant might therefore not reflect the actual distance from the implant *in vivo*.

1 and Ta-2 – *PDO*). Further away from the implant, the predominant orientation was parallel to the surface of the implant in Ta-1 (Fig. 5: Ta-1 – *PDO*), while it was perpendicular to the implant in Ta-2 (Fig. 5: Ta-2 – *PDO*). The mean *PDO* was 27.0 ± 15.5% (mean ± SD) and 26.2 ± 15.2% for Ta-1 and Ta-2, respectively (Table 1).

T was generally higher in Ta-1 (2.49 ± 0.10 nm (mean ± SD)) than in Ta-2 (2.34 ± 0.11 nm) (*t*-test: $p<0.0001$) (Fig. 5: Ta-1 and Ta-2 – *T* and Table 1). However, the smallest *T*-values were found towards the implant surfaces in both regions. In area Ta-1, α was between 1.9 and 2.5, with the highest values found towards positions removed by the filter based on the integrated SAXS intensity (Fig. 5: Ta-1 – α); an influence from the surrounding matrix cannot be ruled out. The magnitude of α was similar in Ta-2 (2.0 ± 0.1 (mean ± SD)) (Table 1). As in the Ti implant sample the smallest values of the shape parameter, around 1.8, was found at the positions with the highest *T* (Fig. 5: Ta-1) (linear regression analysis: Ta-1; R = -0.35, $P<0.0001$. Ta-2; R = -0.59, $P<0.0001$).

Figure 6 shows the average *PDO* and *T* as a function of distance from the implant. In Ta-1, low *PDO* values were found both close to the implant and further away from the implant with values of 23.7 ± 2.9 % (average ± SEM) and 25.1 ± 4.7 %, respectively (Fig. 6A). In between, higher values around 31 % were found. In Ta-2, a significant linear increase in *PDO* from 23.5 ± 2.1 % close to the implant to 41.4 ± 3.8 % 500 – 550 µm from the implant (R = 0.9, $P<0.0001$) was found (Fig. 6B). In both regions, the crystallite thickness, *T*, increased linearly with distance from the implant. In Ta-1 the increase in *T* was from 2.43 ± 0.01 nm (average ± SEM) to 2.58 ± 0.11 nm over a distance 0 to 350 µm (linear regression analysis: R = 0.98, $P<0.0001$), (Fig. 6C), while in Ta-2 the increase was from 2.24 ± 0.01 nm to 2.48 ± 0.05 nm from the implant and 550 µm into the bone (linear regression analysis: R = 0.98, $P<0.0001$) (Fig. 6D).

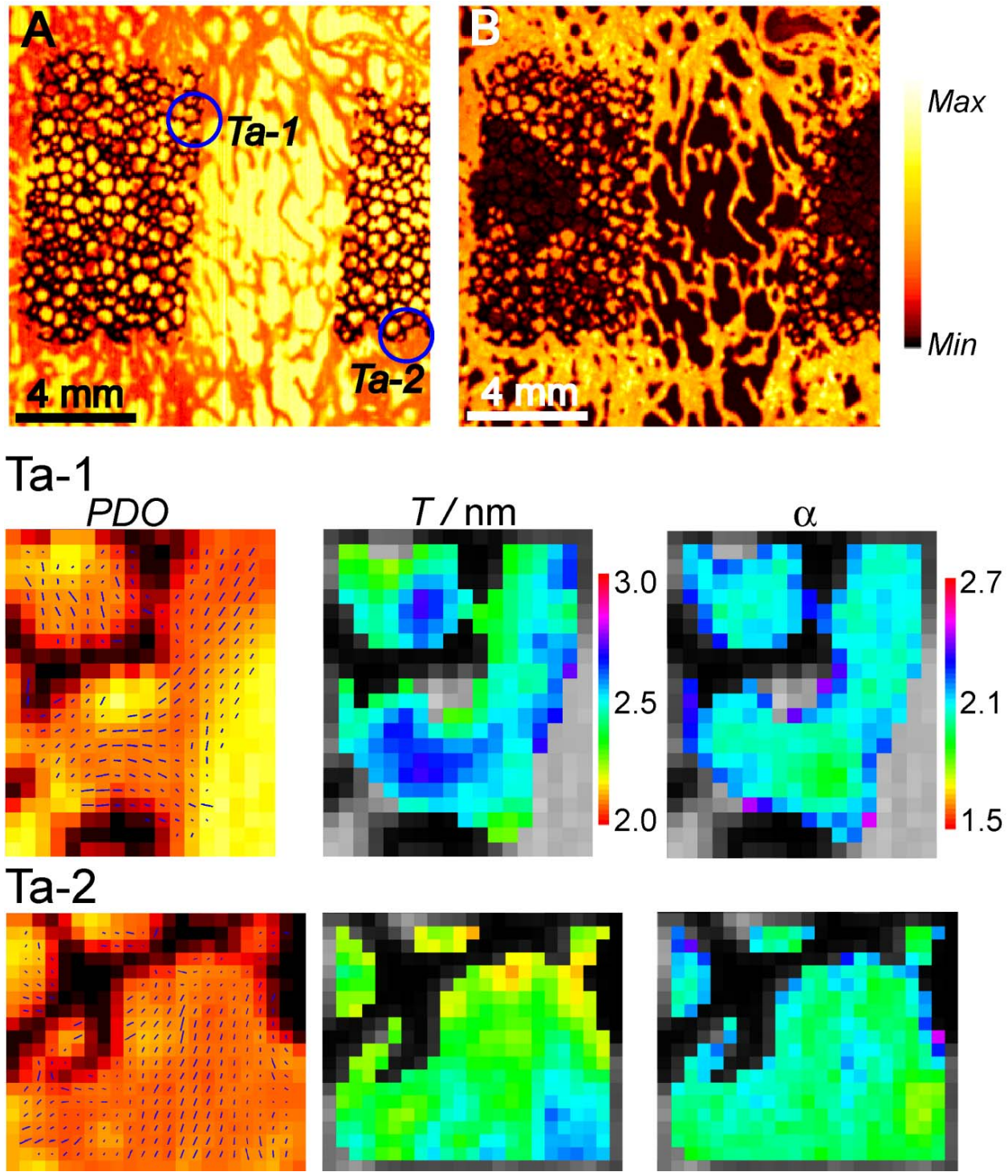

Figure 5. sSAXS images of the Ta implant sample. The pixel size is 50 µm in all images. (A) Survey X-ray transmission scan. (B) Survey SAXS intensity scan. Ta-1) and Ta-2): Detailed investigations of the two regions marked in A. *PDO*, *T* and α are all depicted similar as in Figure 2.

Discussion

In the present study we have applied sSAXS to characterize the nanostructure of bone at and around a Ti and a porous Ta implant in a pig anterior lumbar interbody fusion (ALIF) model. The predominant orientation of the mineral crystallites closest to the implant is found to be parallel to the implant surface in all areas investigated, even though the geometry of the implants varies significantly. This indicates that the implant surface influences the orientation of the mineral phase on a nanometer length scale in the 100 µm region closest to the implants. These results are in perfect agreement with previous work by Cedola *et al.*, 2006 that found mineral crystals to be aligned with the surfaces of subcutaneously implanted scaffolds in a non-loaded model in mice (Cedola *et al.*, 2006). The minerals in bone are believed initially to predominantly grow within gaps in the collagen type-I fibrils under influence of non-collageneus molecules (Landis, 1999; Landis *et al.*, 1993). It is therefore likely that the effect of the implant on mineral particle orientation is mediated by alignment of organic

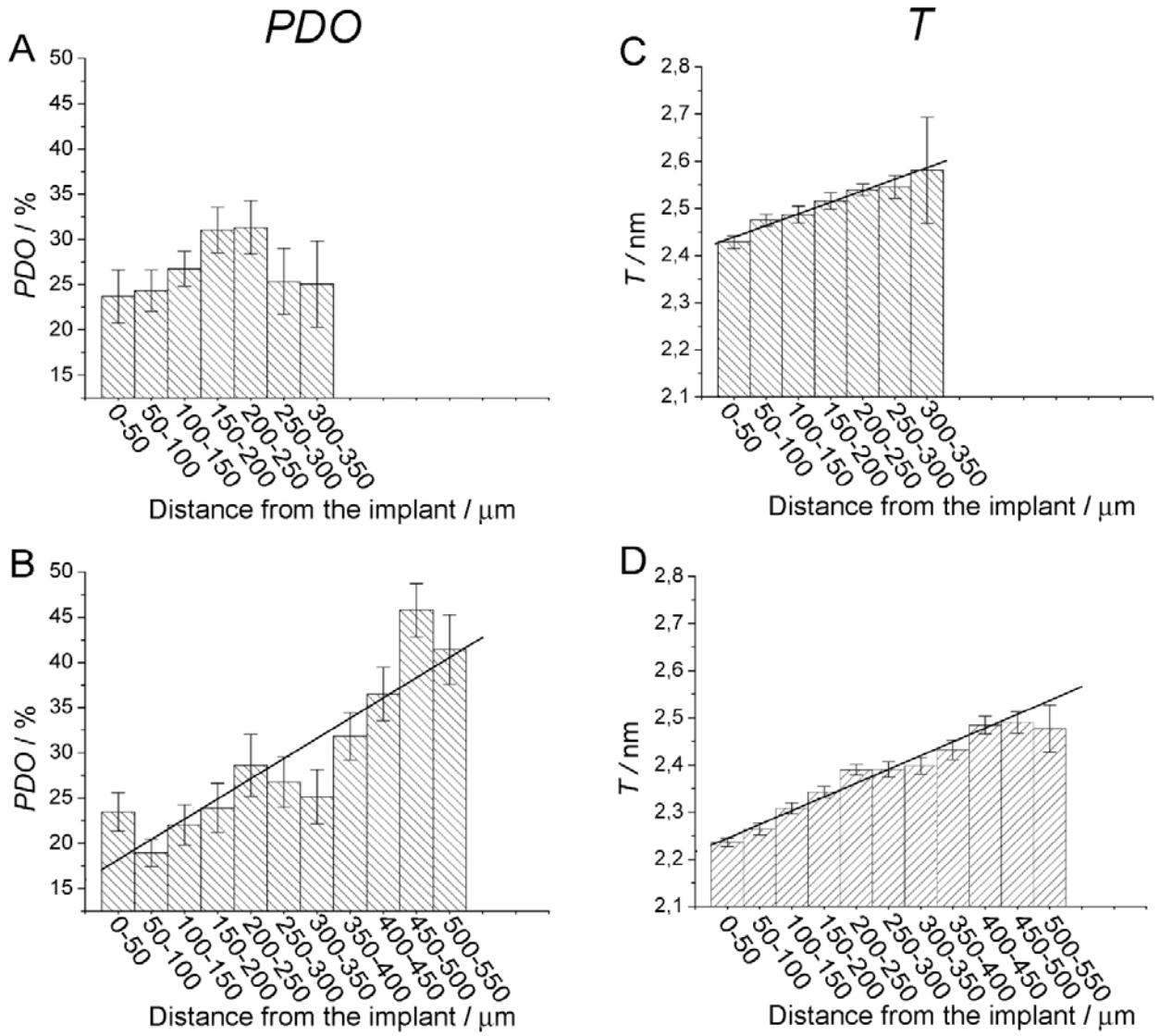

Figure 6. Ta sample. The average *PDO* (A, B) and *T* (C, D) shown as a function of the shortest distance from the implant surface. The solid bars are mean values, while the error bars are the uncertainty around the mean. Trend lines are shown for significant linear correlations ($p < 0.05$). The graphs (A) and (C) represent Ta-1, while (B) and (D) correspond to the region in Ta-2 (Figure 4).

molecules like collagen along the implant surface.

We observed a systematic change in the magnitude of the *PDO* with distance from the implant surface in two out of four regions (Ta-2 and Ti-2), with the lowest values close to the implant (Figs. 4B and 6B). The average magnitude of the *PDO* in the investigated regions ranges from approximately 15 to 45 % and is fully consistent with previous studies (Bünger *et al.*, 2006; Rinnerthaler *et al.*, 1999; Zizak *et al.*, 2003). The low *PDO* found close to the implant can either be explained by the mineral plates being less orientated within the probed volumes or the mineral plates being aligned perpendicular to the plane of the sample. In Ti-1, relatively high values of the averaged *PDO*, around 25-30%, are found next to the implant, followed by a decrease in *PDO* to around 16% 100-150 µm from the surface and an increase to approximately 40 % 600 µm from the surface. These changes in *PDO* coincide very nicely with the change in the predominant orientation. The HA crystals are predominantly aligned along the implant surface in the inner 100 µm zone towards the implant surface. From here the orientation changes into that of the ingrowing bone; it is at this region the low values of the *PDO* is found. Interestingly, small values of the shape parameter, α ~1.6, is also found in this region implying that the nanostructure of the bone is less dense than in the surrounding bone. An interesting open question is whether this zone with low *PDO* and low α values is a mechanically weak point, since it bridges the two mineral orientations with possible low density on the nanometer length scale; however, further studies are required to address this point.

The mean crystal thickness, *T* is between ~ 2.0 and 3.0 nm. This is in perfect agreement with previous SAXS findings where mineral thicknesses of 2–4 nm have been found in human vertebral bone (Rinnerthaler *et al.*, 1999; Zizak *et al.*, 2003) and values between ~2.0 to ~3.5 nm in six-month-old pig bone (Bünger *et al.*, 2006). In both samples, most values of α are between 1.6 and 2.4, which is slightly lower than in previous work on pig bone where values between 2 and 3 were found (Bünger *et al.*, 2006). α reflects the dimensionality and arrangement of crystallites in the bone. For needle-shaped and plate-like

particles α is 1 and 2, respectively (Poon and Haw, 1997). For non-integer values, the higher the value of α (below 3), the more dense and space filling is the arrangement of the crystallites. Therefore, we suggest that the crystallites observed in the present study range from needle-like crystallites with a fractal surface to plate-like crystals. Furthermore, the crystallites are arranged in a network that is less dense than in our previous growth plate study (Bünger *et al.*, 2006). Note that no correlation was found between α and *T* in any of the investigated regions. This means that bone with thick mineral crystals not necessarily has a structure that is more dense or space filling at the nanometer length scale.

Interestingly, we observed a significant increase in crystal thickness *T* with distance from the implant in both regions in the Ta sample (Figs. 6C and 6D) and in the region inside the central hole of the Ti implant (Fig. 4D – Ti-2). In the pig neurocentral growth plate, we have observed an increase in *T* as a function of distance from the growth plate in a similar study (Bünger *et al*., 2006). In that case, we suggested that *T* reflects the age of the bone. The findings in the present study are comparable to the magnitude and the increase in *T* in our growth plate study. It is possible that *T* also reflects the age of the bone in the present study, thereby revealing important information about how the bone grows onto the implant surface. This suggests that the youngest bone is found nearest to the implant surface in Ti-2, Ta-1 and Ta-2. In Ti-1 the situation is different and the highest values of *T* (around 2.7–2.8 nm) are found towards the implant surface (Fig. 3: Ti-1 - *T*). Interestingly, at these positions small values of the shape parameter around 1.7 are found (Fig. 3: Ti-1 – α). This indicates that the shape and arrangement of crystals in the region close to the implant are less dense from what is found in the surrounding bone, where higher values of the shape parameter are determined. It is likely that the implant plays an important role for the formation of bone with the combination of large *T* and small α values. However, high values of *T* associated with low values of the shape parameter are also observed in the Ta sample (Fig. 5 – Ta-2). In contrast to Ti-1 the positions in Ta-2 are found further away from the implant. It is possible that these two regions of bone share ultra-structural properties, despite the fact that they are located at different positions with different distances from the implant.

We observed a marked difference in *T* behaviour as a function of distance from the implant between Ti-1 and Ti-2. *In situ,* the implants are inserted between two adjacent vertebral bodies of the spine. Thus, the implants are predominantly affected by a mechanical load in the axial direction of the vertebral spine due to the weight of the body (Smit, 2002). The overall mechanical load on the two implants is similar, because the weight of the pigs is within the same range (~50 kg at surgery). However, as the Ti implant is much stiffer than bone a mechanical mismatch occurs at the bone-implant interface (Waite *et al.*, 2004). *In vivo*, the mechanical mismatch will give rise to interfacial stresses, which in turn affect the bone tissue in the contact zone between bone and implant. The interfacial stress depends on the difference in stiffness between implant and bone and to the magnitude of the mechanical load. In Ti-2 the *T* parameter increases linearly, while in Ti-1 high values are found at the implant surface. We propose that this difference originates from a difference in interfacial stress near the implant surface caused by lower mechanical load in the central hole of the implant originating from stress shielding. We find a linear increase in *T* as for Ti-2 at both Ta-1 and Ta-2, with higher values in Ta-1 than Ta-2. The stiffness of the porous Ta material is much like that of trabecular bone (Bobyn *et al.*, 1999) resulting in a small mechanical mismatch between implant and bone. Therefore, compared to the Ti implant, lower interfacial stresses are likely to be found in regions subjected to the same mechanical load. It is possible that the reason why we observe an increase in *T* with distance from the implant in both Ta-1 and Ta-2 is because of low interfacial stresses between bone and implant. Furthermore, the similar increase in *T* at the two positions leads us to suggest that the Ta implant does not provide any significant stress shielding from the overall mechanical load at region Ta-2. The Ta implant thereby provides similar conditions for bone in-growth within the central hole of the implant and at the end of the implant. Interestingly, the behaviour in *T* at Ta-1 and Ta-2 resembles that of region Ti-2 in Ti implant. One explanation of this similarity could be that the interfacial stresses at these different positions are the same. It is possible that the connection between *T* and interfacial stress is controlled by cells like osteoblasts that secrete molecules responsible for nucleation and growth of the HA-crystals. However, further studies are needed to shed light on this hypothesis.

Table 1

		Ti-1	Ti-2	Ta-1	Ta-2
n		273	173	213	281
<*PDO*>	*Mean*	27.0	34.1	27.0	26.2
	SD	16.4	15.1	15.5	15.2
	Min	0.2	2.7	1.6	<0.1
	Max	99.1	80.7	78.5	80.8
<*T*>/*nm*	*Mean*	2.50	2.43	2.49	2.34
	SD	0.17	0.16	0.10	0.11
	Min	2.27	2.14	2.24	2.11
	Max	3.10	2.76	2.73	2.60
<α>	*Mean*	1.8	2.0	2.1	2.0
	SD	0.1	0.1	0.1	0.1
	Min	1.6	1.8	1.9	1.8
	Max	2.2	2.2	2.5	2.5

In conclusion, the mineral crystals closest to the implant surface tended to be aligned with the implant surface, possible following the direction of collagen fibres on the implant surface. Detailed scans of two regions in the porous Ta sample and in one region in the Ti sample, revealed a gradient in *T* with the smallest values toward the implant surface. In the second region of the Ti sample the thickest mineral crystals were found towards the implant surface. The observed differences in mineral thickness with distance from the implant surfaces might be explained by differences in mechanical load induced by the implant material and geometrical design. The results demonstrate

the usefulness of the SAXS technique for the investigation of the interaction between implant and bone.

Acknowledgements

The authors thank Annette Milton for technical assistance with histology and the Danish Institute of Agricultural Sciences, Research Center Foulum, for excellent cooperation. We acknowledge financial support from the Danish Research Council through the "Large Interdisciplinary Research Group - Nanoscience & Biocompatibility" (2052-01-0006), the European Commission (FP6 STREP project: NANOCUES), the Novo Nordisk Foundation, and the iNANO Center. Furthermore, we are grateful for financial support from Implex Corporation in the United States, the Danish Rheumatism Association and the Institute of Experimental Clinical Research, University of Aarhus, Denmark. Hedrocel ALIF devices (Porous Ta Implants) were manufactured and kindly provided by Zimmer Inc., Warsaw, IN, USA (previously called Implex Corp.). H.B. gratefully acknowledges financial support from the Danish Natural Sciences Research Council and the Danish Research Council for Technology and Production through a Steno Research Assistant Professor fellowship.

References

Albrektsson T, Johansson C (2001) Osteoinduction, osteoconduction and osseointegration. Eur Spine J **10**: 96-101.

Bobyn JD, Toh KK, Hacking SA, Tanzer M, Krygier JJ (1999) Tissue response to porous tantalum acetabular cups: a canine model. J Arthroplasty **14**: 347-354.

Bobyn JD (1999) Fixation and bearing surfaces for the next millennium. Orthopedics **22**: 810-812.

Bobyn JD, Stackpool GJ, Hacking SA, Tanzer M, Krygier JJ (1999) Characteristics of bone ingrowth and interface mechanics of a new porous tantalum biomaterial. J Bone Joint Surg Br **81**: 907-914.

Bobyn JD, Poggie RA, Krygier JJ, Lewallen DG, Hanssen AD, Lewis RJ, Unger AS, O'Keefe TJ, Christie MJ, Nasser S, Wood JE, Stulberg SD, Tanzer M (2004) Clinical validation of a structural porous tantalum biomaterial for adult reconstruction. J Bone Joint Surg Am **86**: 123-129.

Bünger MH, Foss M, Erlacher K, Hougaard MB, Chevallier J, Langdahl B, Bünger C, Birkedal H, Besenbacher F, Pedersen JS (2006) Nanostructure of the neurocentral growth plate: Insight from scanning small angle x-ray scattering, atomic force microscopy and scanning electron microscopy. Bone **39**: 530-541.

Cedola A, Mastrogiacomo M, Burghammer M, Komlev V, Giannoni P, Favia A, Cancedda R, Rustichelli F, Lagomarsino S (2006) Engineered bone from bone marrow stromal cells: a structural study by an advanced x-ray microdiffraction technique. Phys Med Biol **51**: N109–N116

Fratzl P (1994) Statistical model of the habit and arrangement of mineral crystals in the collagen of bone. J. Statist Phys **77**: 125-143.

Fratzl P, Fratzl-Zelman N, Klaushofer K, Vogl G, Koller K (1991) Nucleation and growth of mineral crystals in bone studied by small-angle X-ray scattering. Calcif Tissue Int 48: 407-413.

Fratzl P, Groschner M, Vogl G, Plenk H, Jr., Eschberger J, Fratzl-Zelman N, Koller K, Klaushofer K (1992) Mineral crystals in calcified tissues: a comparative study by SAXS. J Bone Miner Res **7**: 329-334.

Fratzl P, Schreiber S, Klaushofer K (1996). Bone mineralization as studied by small-angle x-ray scattering. Connect Tissue Res **34**: 247-254.

Gefen A (2005). Review of "The Physical Measurement of Bone" (Langton CM, Njeh CF, eds) Biomed Eng Online **4**: 37.

Landis WJ (1999) An overview of vertebrate mineralization with emphasis on collagen-mineral interaction. Gravit Space Biol Bull **12**: 15-26.

Landis WJ, Song MJ, Leith A, McEwen L, McEwen BF (1993) Mineral and organic matrix interaction in normally calcifying tendon visualized in three dimensions by high-voltage electron microscopic tomography and graphic image reconstruction. J Struct Biol **110**: 39-54.

Li H, Zou X, Woo C, Ding M, Lind M, Bunger C (2005) Experimental anterior lumbar interbody fusion with an osteoinductive bovine bone collagen extract. Spine **30**: 890-896.

Li H (2004) The influence of intervertebral disc tissue on anterior interbody spinal fusion – *In vitro* studies with osteoblast cells and an *in vivo* study in pigs. Dan Med Bull **51**: 304.

Lindner P, Zemb T (eds) (2002) Neutrons, X-rays and Light: Scattering Methods Applied to Soft Condensed Matter: London: Elsevier Science.

Mann S (2002) Biomineralization. Principles and Concepts in Bioinorganic Materials Chemistry. Oxford: Oxford University Press.

Melsen F, Steiniche T (1993) Bone histomorphometry. Osteoporos Int **3**: 98-99.

Pedersen JS (2004) A flux- and background-optimized version of the NanoSTAR small-angle X-ray scattering camera for solution scattering. J Appl Crystallogr **37**: 369-380.

Poon WCK, Haw MD (1997) Mesoscopic structure formation in colloidal aggregation and gelation. Adv Colloid Interface Sci **73**: 71-126.

Rinnerthaler S, Roschger P, Jakob HF, Nader A, Klaushofer K, Fratzl P (1999) Scanning small angle X-ray scattering analysis of human bone sections. Calcif Tissue Int **64**: 422-429.

Smit TH (2002) The use of a quadruped as an in vivo model for the study of the spine – biomechanical considerations. Eur Spine J **11**: 137-144.

Waite JH, Lichtenegger HC, Stucky GD, Hansma P (2004) Exploring molecular and mechanical gradients in structural bioscaffolds. Biochemistry **43**: 7653-7662.

Young MF (2003). Bone matrix proteins: their function, regulation, and relationship to osteoporosis. Osteoporos Int **14**: 35-42.

Zizak I, Roschger P, Paris O, Misof BM, Berzlanovich A, Bernstorff S, Amenitsch H, Klaushofer K, Fratzl P (2003) Characteristics of mineral particles in the human bone/cartilage interface. J Struct Biol **141**: 208-217.

Zou X, Li H, Bunger M, Egund N, Lind M, Bunger C (2004) Bone ingrowth characteristics of porous tantalum and carbon fiber interbody devices: an experimental study in pigs. Spine J **4**: 99-105.

Zou X, Li H, Teng X, Xue Q, Egund N, Lind M, Bunger C (2005) Pedicle screw fixation enhances anterior lumbar interbody fusion with porous tantalum cages: an experimental study in pigs. Spine **30**: 392-399.

Discussion with Reviewers

Reviewer I: In the future it could be very interesting to further investigate the issue, opened by the present paper, regarding the relation between the crystal thickness and the mechanical load. In this regard the results should be considered, which were obtained in the case of engineered bone (Cedola *et al*., 2006) grown on the pore surface of a ceramic scaffold. In this case the scaffold was implanted subcutaneously on the neck of the animal (almost zero mechanical load) and the crystals, oriented parallel to pore surface, decrease their thickness linearly with the distance from the scaffold surface.

Authors: We fully agree with the reviewer that the relationship between mechanical load and crystal thickness and orientation in bone is a very interesting subject and deserves attention in future studies. Several factors on different length scales, including for example the external mechanical load, local environment at the site of bone formation and properties (mechanical, structural and chemical) of the substrate/implant may potentially influence the growth and orientation of the mineral crystals in the forming bone. In the study by Cedola *et al*. (2006) collagen fibres and mineral crystals were aligned parallel to the scaffold surface in a non-loaded model. Our results are consistent with these findings and underline the important role of the implant/scaffold in the orientation of collagen fibers and mineral crystals.

T. Wess: The α parameter needs to be discussed in more detail: this seems to have a similar information content to the η parameter used by Fratzl where the deviation from a Lorenzian profile gives some information on shape.

Authors: Our shape parameter and Fratzl's η parameter reflect the same physics. The parameters are both related to the shape and arrangement of mineral crystals and molecules in bone. The magnitude of both parameters is independent of the thickness parameter. However, we have looked into the original literature and not been able to identify a simple relationship between the two parameters. We decided on using our approach because we feel that the fractal description used by us is more general concept, which can be used also when concentration effects are present.

T. Wess: I would like the authors to comment on the fact that their authors approach to estimation of crystallite thickness assumes that the volume fraction is constant and 50%. This is the value '4' in the formula quoted.

Authors: The thickness parameter, T, is a good approximation of the mean mineral thickness in bone if it is assumed that the mineral crystals are plate shaped and the volume fraction of minerals in bone does not deviate significantly from 50 %. As described by Zizak *et al.* (2003) the value of *T* depends on the volume fraction of the two phases in the sample by the equation

$$T = 4\phi(1-\phi)/\sigma , \qquad (1)$$

where ϕ is the volume fraction of the mineral crystals and σ is the surface area of the minerals per unit volume bone. If there is no particle agglomeration, equation (1) can also be written as

$$T = 2(1-\phi)/(1/a+1/b+1/c), \qquad (2)$$

where *a*, *b* and *c* are the plate dimensions (Zizak *et al.*, 2003). If the minerals are plate shaped with $a<<b, c$, then *T* is

$$T = 2(1-\phi)a, \qquad (3)$$

If the volume fraction of the two phases deviates significantly from 50%, a systematic error is introduced. For say a volume fraction of 45%, *T* will be 10% larger than *a*.

In human trabecular bone the volume fractions of minerals have previously been estimated by quantitative backscatter electron imaging (qBSEI) to be approximately 35-40% (Roschger *et al.*, 1998). If the samples in the present study have a mineral volume fraction similar to these values from human bone, it is possible that our *T* values are systematically too low. In most of the literature, however, *T* values that have not been corrected for mineral volume fraction are reported and it therefore seemed most appropriate to report the uncorrected *T* values.

A large variation in the mineral volume fraction within the sample could be a problem in large scanning SAXS experiments if one is to look for trends within a sample. Small differences in *T* could be due to regional differences in the bone mineral volume fraction. However, the variation in mineral volume fraction within bone samples has previously been demonstrated to below approximately 5% (Zizak *et al.*, 2003), which leads to smaller differences in *T* than what we observe in the present study. Considering the full span estimated by Roschger *et al*. (1998) we obtain for ϕ=40% and 30%, respectively: T=1.2a and T=1.3a. This leads to a maximal phase fraction induced variation of *T* of ΔT_{max} = (1.2-1.3)/1.3 = 7.7%, which is smaller than the span of *T*-values measured. To test for correlations between phase fraction and *T*, we plotted *T* as a function of the relative transmission of the sample as measured in the survey scans. The latter is a function of the effective bone thickness and the phase fraction and thus not a direct measure of ϕ, but the best one available in the present case, where the sample thickness is comparable to the thickness of a single trabecula. We found no apparent correlation between transmission and *T* lending some support to the notion that the variations in ϕ are not dominant.

Finally, we wish to add that one potential difficulty in using qBSEI to correct for variations in mineral volume fraction is that this technique only probes the exposed surface layer and not the full thickness of the sample, which is what is sampled by SAXS.